Available online at www.sciencedirect.com

ScienceDirect

journal homepage: www.elsevier.com/locate/he

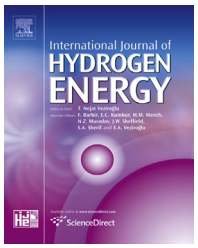

Effect of Pr^{3+}/Pr^{4+} ratio on the oxygen ion transport and thermomechanical properties of the pyrochlore and fluorite phases in the ZrO_2–Pr_2O_3 system

A.V. Shlyakhtina [a,*], J.C.C. Abrantes [b,c], E. Gomes [c], A.N. Shchegolikhin [d], G.A. Vorobieva [a], K.I. Maslakov [e], A.V. Knotko [e], L.G. Shcherbakova [a]

[a] Semenov Institute of Chemical Physics, Russian Academy of Sciences, Moscow, 119991, Russia
[b] UIDM, ESTG, Instituto Politécnico de Viana do Castelo, Apartado 574, Viana do Castelo, 4901-348, Portugal
[c] Aveiro Institute of Materials–CICECO (DEMAC), University of Aveiro, Aveiro, 3810, Portugal
[d] Emanuel Institute of Biochemical Physics, Russian Academy of Sciences, ul. Kosygina 4, Moscow, 119991, Russia
[e] Faculty of Chemistry, Moscow State University, Leninskie gory 1, Moscow, 119991, Russia

ARTICLE INFO

Article history:
Received 22 September 2015
Received in revised form
25 February 2016
Accepted 29 February 2016
Available online 1 April 2016

Keywords:
Pyrochlore
Fluorite
Oxygen ion conductivity
Electronic conductivity
Thermomechanical properties

ABSTRACT

This paper examines the effect of the Pr^{3+}/Pr^{4+} ratio on the mechanism of ionic and electronic transport in the $(Pr_{2-x}Zr_x)Zr_2O_{7+x/2}$ ($x = 0.15$), $Pr_2Zr_2O_7$, and $Pr_2(Zr_{2-x}Pr_x)O_{7-x/2}$ ($x = 0.1$) pyrochlore phases and Pr_3ZrO_x with the fluorite structure and on the behavior of their thermal expansion coefficient (TEC). The solid solutions were prepared through coprecipitation followed by firing of the green compacts in air at a high temperature of 1550 °C for 4 h. The Pr^{3+}/Pr^{4+} ratio was shown to decrease in going from the $(Pr_{2-x}Zr_x)Zr_2O_{7+x/2}$ ($x = 0.15$), $Pr_2Zr_2O_7$, and $Pr_2(Zr_{2-x}Pr_x)O_{7-x/2}$ ($x = 0.1$) pyrochlores to the Pr_3ZrO_x fluorite, leading to changes in the conductivity type from mixed (ionic–electronic) to electronic and in the color of the materials from beige to black and to an anomalous deviation of the TEC from linearity in fluorite Pr_3ZrO_x, i.e. at the highest Pr^{4+} content. According to impedance spectroscopy results, $(Pr_{2-x}Zr_x)Zr_2O_{7+x/2}$ with $x = 0.15$ has purely oxide-ion conductivity (3×10^{-3} S/cm at 1000 °C) in a wide range of oxygen partial pressures: from 10^{-10} to 10^2 Pa. With increasing Pr content, p-type electronic conductivity becomes significant, reaching a maximum in fluorite Pr_3ZrO_x: ~0.5 S/cm at 1000 °C. According to XPS data, all pyrochlore samples $(Pr_{2-x}Zr_x)Zr_2O_{7+x/2}$ ($x = 0.15$), $Pr_2Zr_2O_7$ and $Pr_2(Zr_{2-x}Pr_x)O_{7-x/2}$ ($x = 0.1$) contain only Pr^{3+} at room temperature, whereas Pr_3ZrO_x contains both Pr^{3+} and Pr^{4+}. The considerable deviation of the TEC of Pr_3ZrO_x from linearity above 500 °C is due to partial reduction of Pr^{4+}. The reduction process $Pr^{4+} + e' \rightarrow Pr^{3+}$ followed by oxygen release in the range 500–1100 °C has been identified in Pr_3ZrO_x by thermal analysis and mass spectrometry in a He atmosphere.

* *Corresponding author*. Tel.: +7 495 9397950; fax: +7 499 2420253.
E-mail addresses: annashl@inbox.ru, annash@chph.ras.ru (A.V. Shlyakhtina).
http://dx.doi.org/10.1016/j.ijhydene.2016.02.152

Introduction

Many undoped and acceptor-doped $Ln_2M_2O_7$ (Ln = La–Lu; M = Ti, Zr, Hf) pyrochlores are widely known oxygen vacancy conductors. Oxygen vacancy generation in these materials has been extensively discussed in the literature [1–10]. Their main potential application is solid electrolytes for SOFCs because they are close in oxide ion conductivity to the conventional ZrO_2-based solid electrolytes doped with 10–15 mol % Y_2O_3 or Sc_2O_3 [11]. Among the pyrochlore zirconates, the $Ln_2Zr_2O_7$ (Ln = Ce, Pr) zirconates, containing 3+/4+ variable-valence cations (Ce and Pr) are the least studied. The main reason for this is that during synthesis in air the Ln^{3+} in the $Ln_2Zr_2O_7$ (Ln = Ce, Pr) pyrochlores as a rule partially oxidizes to Ln^{4+} [12–15], which leads to coexistence of the Ln^{3+} and Ln^{4+} in the A site of $Ln_2Zr_2O_7$ pyrochlores:

$$Ln^{3+} + h^{\bullet} \leftrightarrow Ln^{4+}. \quad (1)$$

This process limits the use of these pyrochlores as solid electrolytes, but they can be studied as MIECs for SOFC electrodes.

The Pr and Tb cations are the most stable in the pyrochlore structure among the known 3+/4+ variable-valence rare-earth cations [16]. In particular, $Tb_2Ti_2O_7$ and $Tb_2Hf_2O_7$ can be synthesized readily in air and the only compound in the Tb_2O_3–ZrO_2 system is fluorite $Tb_2Zr_2O_7$ ($TbZrO_{4-\delta}$) [17,18]. $Pr_2Zr_2O_7$ can be prepared rather easily both by solid-state reaction and using solution techniques followed by high-temperature firing in air [15,19,20]. Undoped $Ce_2Zr_2O_7$ can only be synthesized under reducing conditions, and subsequent exposure of this material to air leads to the oxidation of Ce^{3+} to Ce^{4+} [13,14]. Thus, because of the low potential of $Ce^{3+} \rightarrow Ce^{4+}$ oxidation (1.44–1.7 V), $Ce_2Zr_2O_7$ cannot be used as a SOFC material.

It should be emphasized that ionic and electronic transport processes in the Pr_2O_3–ZrO_2 system have been the subject of a limited number of reports [15,19–22]. In connection with this, studies of $Pr_xCe_{1-x}O_{2-\delta}$ (x = 0, 0.01, 0.1, 0.2) as potential SOFC cathodes [23–25] are of interest, where the oxide ion conductivity was measured as a function of oxygen partial pressure, the thermomechanical behavior of the materials was investigated, and anomalous thermal expansion was found at temperatures $T > 500$–600 °C in air, which was tentatively attributed to the reduction of Pr^{4+} to Pr^{3+} at these temperatures. This was accompanied by a considerable rise in electronic conductivity at elevated temperatures.

Because of this, we investigated not only the conductivity (as a function of oxygen partial pressure) but also the thermomechanical properties of pyrochlore-like Pr_2O_3–ZrO_2 solid solutions in the rather narrow (~6 mol %) isomorphous miscibility range of $Pr_{2\pm x}Zr_{2\pm x}O_{7\pm\delta}$ and those of a Pr-rich fluorite solid solution.

The following compositions were studied:

pyrochlore $(Pr_{2-x}Zr_x)Zr_2O_{7+x/2}$ (x = 0.15), containing excess Zr^{4+} on the Pr^{3+} site, as a potential interstitial conductor, in which the formation of oxygen interstitials can be represented (in Kröger–Vink notation) by Eq. 2

$$(2+x)ZrO_2 + (1-x/2)Pr_2O_3 \rightarrow (2-x)Pr_{Pr}^{x} + xZr_{Pr}^{\bullet} + 2Zr_{Zr}^{x} + 7O_O^{x} + x/2O_i'' \quad (2)$$

the pyrochlore compound $Pr_2Zr_2O_7$;

pyrochlore $Pr_2(Zr_{2-x}Pr_x)O_{7-x/2}$ (x = 0.1), containing excess Pr^{3+} on the Zr^{4+} site, as a potential oxygen vacancy conductor, in which oxygen vacancy formation can be described by Eq. 3

$$(2-x)ZrO_2 + (1+x/2)Pr_2O_3 \rightarrow (2-x)Zr_{Zr}^{x} + xPr_{Zr}' + 2Pr_{Pr}^{x} + (7-x/2)O_O^{x} + x/2V_O^{\bullet\bullet} \quad (3)$$

and a $Pr_2(Zr_{2-x}Pr_x)O_{7-x/2}$ (x = 1) Pr-rich fluorite solid solution.

Experimental

Using coprecipitation followed by heat treatment at 1550 °C for 4 h, we prepared pyrochlore- and fluorite-like PrZrO solid solutions containing 30, 33.3, 35.5, and 60 mol % Pr_2O_3 [20], which corresponds to the following compositions: $(Pr_{2-x}Zr_x)Zr_2O_{7+x/2}$ (x = 0.15), $Pr_2Zr_2O_7$, $Pr_2(Zr_{2-x}Pr_x)O_{7-x/2}$ (x = 0.1, 1).

The starting chemicals used were $PrCl_3$ and $ZrOCl_2 \cdot 8H_2O$ powders, which were dissolved in distilled water. Solution concentrations were determined gravimetrically. The concentrations of the chloride solutions were 0.09 M (Pr) and 1.085 M (Zr). All the PrZrO solid solutions were synthesized through reverse precipitation (pH 11.6–11.2), by adding titrated praseodymium chloride and zirconium chloride solutions to aqueous ammonia. After the formation of light green gel-like precipitates, they were aged at room temperature for 4 h. Next, the mother liquor was decanted and the rest was centrifuged. The precipitate was washed with warm water five times to remove Cl^- ions and then dried in air for 66 h at 75 °C, which allowed it to remain light green in color, typical of trivalent Pr. The development of a brown color during drying indicates the formation of Pr^{4+} centers.

The hydroxide precursors thus prepared were pressed at 259 (first composition) or 216 MPa (last three compositions) into pellets, which were then fired at 1550 °C for 4 h.

The density of the resultant samples was determined by measuring their mass and dimensions and ranged from 85 to 90% of their X-ray density [20]. All of the synthesized solid solutions were characterized by X-ray diffraction (XRD) on a DRON-3M (filtered CuK_α radiation, step scan mode with a step of 0.05°, angular range $2\theta = 10$–100°, Rietveld refinement).

The oxidation state of the praseodymium in the solid solutions was determined by X-ray photoelectron spectroscopy (XPS) on a Kratos Axis Ultra DLD spectrometer using a monochromatic Al Kα X-ray source (1486.6 eV, 150 W). High-resolution spectra were acquired at 40 eV pass energy. The analysis area was about 300 × 700 μm. The binding energy scale of the spectrometer was preliminary calibrated using the following lines of standards (cleaned by ion sputtering): Au $4f_{5/2}$ at 83.96 eV, Cu $2p_{3/2}$ at 932.62 eV, and Ag $3d_{5/2}$ at 368.21 eV. A Kratos charge neutralizer system was used. As the binding-energy-scale reference, we used the C 1s level (284.6 eV) arising from the carbon adsorbed on the sample surface.

Thermal analysis was carried out using a Netzsch STA 449C system in combination with an AEOLOS-32 mass

spectrometer between 25 and 1100 °C in helium atmosphere containing a small percentage of oxygen.

Thermomechanical analysis (TMA) curves were recorded in the range of 20–800 °C with the aid of a Perkin-Elmer TMA 7 analyzer equipped with a standard flat-tip probe. The samples in the form of pressed and prepolished disks (~2 mm thickness, ~6 mm dia.) were run at a heating rate of 5 K/min by using a TMA probe load of 100 mN. All the acquired TMA curves were processed using the NETZSCH-Proteus TA software package (v. 4.8.4). Only the TMA curves collected as the result of the second heating run were used for data mining. The physical α curves specifying the linear thermal expansion coefficient (TEC) values of the sample at any given temperature (not shown) were automatically calculated with NETZSCH-Proteus TA by the following equation: $\alpha_1(T) = 1/L_0$ (dL/dT), where L_0 is the sample length (disk thickness) at the beginning of the TMA experiment (20 °C). Some TEC values taken at discrete temperatures are given in Table 3. The TEC transition onset temperatures were determined graphically from the abscissa intercepts of the tangents drawn on the two sides of the TMA peak (below and above the transition temperature).

Conductivity was measured in air between 300 and 750 °C and as a function of oxygen partial pressure (between 700 and 1000 °C) during reoxidation and after reduction with a mixture of 95% N_2 and 5% H_2. A potentiometric oxygen sensor was used to monitor the oxygen partial pressure during the slow reoxidation process. Both pellet faces were coated with Pt paste (Engelhard) and the pellets were fired at 1000 °C for 30 min in order to obtain electrodes of lateral resistance < 1 Ω. The electrical measurements, both in a reducing atmosphere and in air, were made by impedance spectroscopy in the frequency range of 20 Hz–1 MHz, with a signal level between 100 and 250 mV (higher levels only at low temperature to avoid noise due to high resistance of the sample) using a Hewlett-Packard 4284A precision LCR bridge. The measurements of conductivity as a function of the oxygen partial pressure were performed only at high temperatures (700–1000 °C) due to oxygen sensor limitations. At these conditions the impedance spectra only present a single arc, attributed to the electrode reaction, or a single point over the x-axis, which corresponds to the total resistance of the sample.

Results and discussion

Structure of the $(Pr_{2-x}Zr_x)Zr_2O_{7+x/2}$ (x = 0.15), $Pr_2Zr_2O_7$, and $Pr_2(Zr_{2-x}Pr_x)O_{7-x/2}$ (x = 0.1) pyrochlores and $Pr_2(Zr_{2-x}Pr_x)O_{7-x/2}$ (x = 1) fluorite studied by XRD: Rietveld refinement

Previously, Belov et al. [20] reported XRD data for the pyrochlore solid solutions under consideration. Here, we present XRD Rietveld refinement results for the same pyrochlore samples: $(Pr_{2-x}Zr_x)Zr_2O_{7+x/2}$ (x = 0.15), $Pr_2Zr_2O_7$, $Pr_2(Zr_{2-x}Pr_x)O_{7-x/2}$ (x = 0.1) and $Pr_2(Zr_{2-x}Pr_x)O_{7-x/2}$ (x = 1) fluorite (slow and fast cooling from 800 °C) (Fig. 1, a, b, c, d, e).

Tables 1 and 2 present Rietveld refinement results for all the pyrochlores. The percentages of cation antisite defects, antistructure pairs and occupancies of different oxygen positions are indicated in Table 1. Our results (Tables 1 and 2) demonstrate that, like $Nd_2Zr_2O_7$ [26,27], $Pr_2Zr_2O_7$ has an ordered pyrochlore structure. This is obviously due to the rather large difference in ionic radius between $Pr^{3+}_{CN=8}$ (1.126 Å) and $Zr^{4+}_{CN=6}$ (0.72 Å). The structure of the $Pr_2(Zr_{2-x}Pr_x)O_{7-x/2}$ (x = 1) Pr-rich solid solution (Fig. 1, d) was shown to be the most similar to the fluorite (CaF_2) structure, with a unit-cell parameter of 5.41874(9) Å, which is close to that of undoped PrO_2: 5.392 Å (JCPDS PDF-2 24-1006). In what follows, we can write its formula as $Pr_2(Zr_{2-x}Pr_x)O_{7-x/2}$ (x = 1) as Pr_3ZrO_x.

XPS determination of the Pr valence state in the $(Pr_{2-x}Zr_x)Zr_2O_{7+x/2}$ (x = 0.15), $Pr_2Zr_2O_7$, and $Pr_2(Zr_{2-x}Pr_x)O_{7-x/2}$ (x = 0.1) pyrochlores and Pr_3ZrO_x fluorite

Arsentiev et al. [16] infer from phase diagram data for the Pr_2O_3–ZrO_2 system in air and vacuum [28–30] that, at large percentages of Pr_2O_3 in mPr_2O_3–$nZrO_2$ mixtures (60 mol % Pr_2O_3 in our case), thermal annealing in an oxidizing atmosphere increases the amount of Pr^{4+}. According to XRD data, the 60% Pr_2O_3 – 40% ZrO_2 (Pr_3ZrO_x) material has the fluorite structure, whereas 30% Pr_2O_3 – 70% ZrO_2, 33.3% Pr_2O_3 – 67.7% ZrO_2 and 35.5% Pr_2O_3 – 64.5% ZrO_2 have the pyrochlore structure.

The pyrochlore structure is known to be a fluorite-related superstructure with a higher degree of order. Fluorites have a loose structure, in which the oxidation state of cations may change, leading to oxygen release or absorption. Thus, the oxygen storage capacity of the fluorite structure exceeds that of the pyrochlore structure. It is for this reason that Pr^{4+} is more readily formed in fluorites, whereas the valence state of praseodymium in pyrochlores is typically 3+.

It seems likely that the Pr^{3+} cation in the cubic fluorite structure (CaF_2) is less stable than in the pyrochlore structure ($(Pr_{2-x}Zr_x)Zr_2O_{7+x/2}$ (x = 0.15) and $Pr_2(Zr_{2-x}Pr_x)O_{7-x/2}$ (x = 0, 0.1)) and that the Pr in $Pr_2(Zr_{2-x}Pr_x)O_{7-x/2}$ with x = 1 (Pr_3ZrO_x) is largely in its tetravalent state, so the formula of the Pr_3ZrO_x solid solution should be written as $Pr_3ZrO_{8-\delta}$.

To determine the Pr^{3+}/Pr^{4+} ratio we analyzed the XPS data for the solid solutions under investigation. The valence of the praseodymium (3+ or 4+) in the $(Pr_{2-x}Zr_x)Zr_2O_{7+x/2}$ (x = 0.15), $Pr_2Zr_2O_7$, and $Pr_2(Zr_{2-x}Pr_x)O_{7-x/2}$ (x = 0.1) pyrochlores and $Pr_3ZrO_{8-\delta}$ fluorite solid solution synthesized through co-precipitation can be accurately determined by XPS. Hea et al. [31,32] and Sinev et al. [33] investigated the XPS spectra of Pr^{3+} and Pr^{4+} in the Pr_2O_3–ZrO_2 [33] and similar systems [31,32] for the powder samples. In this study, ceramic $(Pr_{2-x}Zr_x)Zr_2O_{7+x/2}$ (x = 0.15), $Pr_2Zr_2O_7$, $Pr_2(Zr_{2-x}Pr_x)O_{7-x/2}$ (x = 0.1), and $Pr_3ZrO_{8-\delta}$ samples were characterized by XPS.

Fig. 2 shows the room temperature Pr 3d XPS spectra of the $(Pr_{2-x}Zr_x)Zr_2O_{7+x/2}$ (x = 0.15), $Pr_2Zr_2O_7$, $Pr_2(Zr_{2-x}Pr_x)O_{7-x/2}$ (x = 0.1), and $Pr_3ZrO_{8-\delta}$ solid solutions. The chemical shift ΔE_b of XPS lines is known to correlate with the effective charge on the atoms involved in bonding. Accordingly, the oxidation state of praseodymium is a quasi-linear function of the energy position of the Pr 3d level. This can be used to assess the chemical state of praseodymium in its compounds with oxygen.

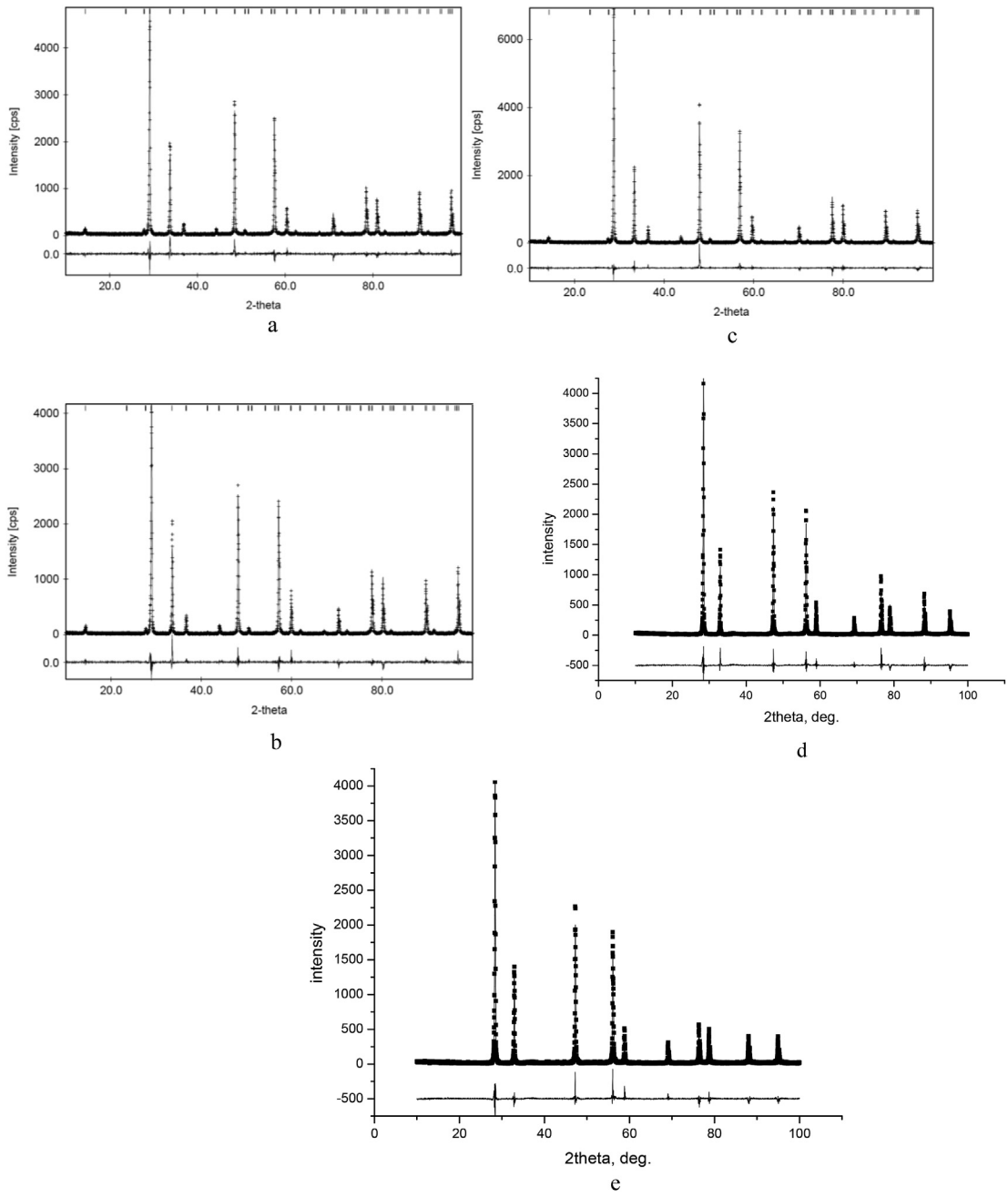

Fig. 1 – XRD Rietveld refinement profiles for the pyrochlore-like (a) $(Pr_{2-x}Zr_x)Zr_2O_{7+x/2}$ (x = 0.15), (b) $Pr_2Zr_2O_7$, (c) $Pr_2(Zr_{2-x}Pr_x)O_{7-x/2}$ (x = 0.1), and (d) fluorite $Pr_2(Zr_{2-x}Pr_x)O_{7-x/2}$ (x = 1) after slow cooling from 800°C, and (e) fluorite $Pr_2(Zr_{2-x}Pr_x)O_{7-x/2}$ (x = 1) after rapid quenching (in liquid N_2) from 800°C.

Table 1 – Compositions and XRD Rietveld refinement results.

Mol. % Pr_2O_3	Formula	$Zr^{\bullet}_{Pr}+Pr'_{Zr}$ antistructure pairs, %	$Zr^{\bullet}_{Pr}$ antisite defects, %	Pr'_{Zr} antisite defects, %	Interstitial oxygen in position 8b	Oxygen vacancy in position 48f	Relation between Pr^{x}_{Pr} and Zr^{x}_{Zr}
30	$(Pr_{2-x}Zr_x)Zr_2O_{7+x/2}$ (x = 0.15)	3	10.5	3	0.08	0	$Pr_{Pr} < Zr_{Zr}$
33.3	$Pr_2Zr_2O_7$ (x = 0)	0	0	0	–	0	$Pr_{Pr} = Zr_{Zr}$
35.5	$Pr_2(Zr_{2-x}Pr_x)O_{7-x/2}$ (x = 0.096)	1.8	1.8	6.58	–	0.008	$Pr_{Pr} > Zr_{Zr}$

Table 2 – Rietveld data for $(Pr_{2-x}Zr_x)Zr_2O_{7+x/2}$ (x = 0.15), $Pr_2Zr_2O_7$, $Pr_2(Zr_{2-x}Pr_x)O_{7-x/2}$ (x = 0.1) synthesized at 1550 °C in 4 h.

Composition	Site	Occupancy	x	y	z	R_{wp} R_p RR Re S D RI RF, %	a, Å
$Pr_{1.85}Zr_{2.15}O_{7.08}$ (30% Pr_2O_3)	Pr_{Pr} (16d)	0.895(4)	0.625	0.625	0.625	15.03	10.6327(1)
	Zr_{Pr} (16d)	0.105	0.625	0.625	0.625	11.19	
	Zr_{Zr} (16c)	0.97	0.125	0.125	0.125	16.14	
	Pr_{Zr} (16c)	0.03	0.125	0.125	0.125	11.13	
	O(1) (8a)	1	0.5	0.5	0.5	1.3503	
	O(2) (48f)	1	0.2143(6)	0	0	1.2178	
	O(3) (8b)	0.08	0.75	0.75	0.75	4.69	
						3.7	
$Pr_2Zr_2O_7$	Pr_{Pr} (16d)	1	0.625	0.625	0.625	16.28	10.7175(1)
	Zr_{Pr} (16d)	0	0.625	0.625	0.625	11.68	
	Zr_{Zr} (16c)	1	0.125	0.125	0.125	15.13	
	Pr_{Zr} (16c)	0	0.125	0.125	0.125	12.18	
	O(1) (8a)	1	0.5	0.5	0.5	1.3375	
	O(2) (48f)	1	0.2026(6)	0	0	1.2336	
						5.24	
						4.59	
$Pr_{2.092}Zr_{1.904}O_{6.952}$ (35.5% Pr_2O_3)	Pr_{Pr} (16d)	0.983(4)	0.625	0.625	0.625	13.96	10.7257(1)
	Zr_{Pr} (16d)	0.018	0.625	0.625	0.625	10.04	
	Zr_{Zr} (16c)	0.934	0.125	0.125	0.125	13.38	
	Pr_{Zr} (16c)	0.066	0.125	0.125	0.125	10.75	
	O(1) (8a)	1	0.5	0.5	0.5	1.2982	
	O(2) (48f)	0.992	0.2050(6)	0	0	1.2588	
						5.3	
						4.16	

Table 3 – Physical expansion coefficient α (TEC) values for some discrete temperatures.

T, °C	Samples			
	$(Pr_{2-x}Zr_x)Zr_2O_{7+x/2}$ (x = 0.15)	$Pr_2Zr_2O_7$	$Pr_2(Zr_{2-x}Pr_x)O_{7-x/2}$ (x = 0.1)	Pr_3ZrO_x
	Phys. α, 1/K x 10^{-6}	Phys. α, 1/K x 10^{-6}	Phys. α, 1/K x 10^{-6}	Phys. α, 1/K x 10^{-6}
50	7.954	8.005	9.446	7.639
100	9.324	11.188	9.448	10.340
150	9.943	10.778	9.672	10.102
200	10.283	11.513	10.270	10.443
250	10.512	10.679	10.500	9.913
300	9.539	10.652	10.828	8.795
350	10.543	10.696	10.264	9.587
400	10.996	11.148	9.889	8.512
450	11.608	11.894	11.254	6.129
500	12.026	12.414	11.192	10.208
550	12.201	12.788	11.827	21.397
600	15.104	14.805	12.515	22.978
650	15.752	15.225	13.669	21.080
700	16.796	17.814	15.385	21.913
750	16.644	18.387	17.348	22.689
800	25.118	17.135	13.305	28.843

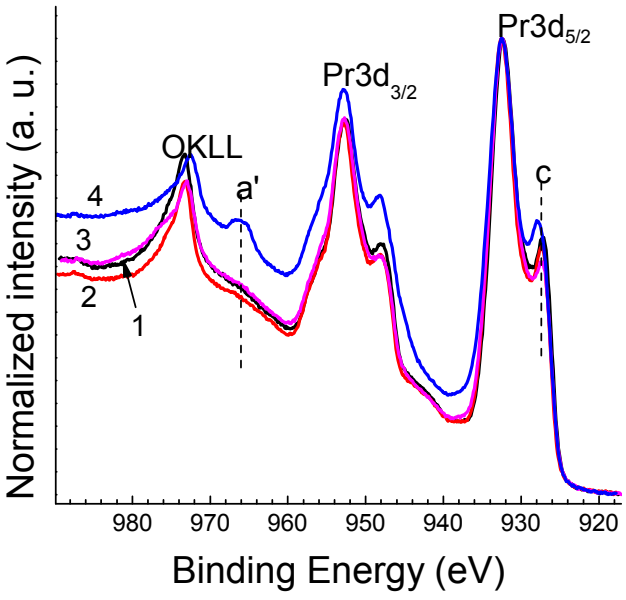

Fig. 2 – Pr 3d XPS spectra for (1) $(Pr_{2-x}Zr_x)Zr_2O_{7+x/2}$ (x = 0.15), (2) $Pr_2Zr_2O_7$, (3) $Pr_2(Zr_{2-x}Pr_x)O_{7-x/2}$ (x = 0.1), and (4) Pr_3ZrO_x solid solutions at room temperature.

The $(Pr_{2-x}Zr_x)Zr_2O_{7+x/2}$ (x = 0.15), $Pr_2Zr_2O_7$, and $Pr_2(Zr_{2-x}Pr_x)O_{7-x/2}$ (x = 0.1) pyrochlore samples have similar spectra, in which line a′, with a binding energy of ~966 eV, is missing (Fig. 2, curves 1–3). This shows that the praseodymium is almost completely in the valence state 3+ in these samples in accordance with [33]. In the spectrum of $Pr_3ZrO_{8-\delta}$, peak a′ is clearly visible, and there is peak c with increased intensity, which indicates the presence of a significant amount of Pr^{4+} (Fig. 2, curve 4). At the same time, the relative intensity of peak a′ is slightly lower than that in the spectrum of PrOy [33]. This indicates that the praseodymium in $Pr_2(Zr_{2-x}Pr_x)O_{7-x/2}$ (x = 1) is in a mixed (3+ and 4+) oxidation state and its formula should be written as Pr_3ZrO_x.

According to XPS analysis data, all the pyrochlore samples $(Pr_{2-x}Zr_x)Zr_2O_{7+x/2}$ (x = 0.15), $Pr_2Zr_2O_7$ and $Pr_2(Zr_{2-x}Pr_x)O_{7-x/2}$ (x = 0.1) synthesized at 1550 °C in air contain only Pr^{3+} at room temperature, whereas Pr_3ZrO_x fluorite contains both Pr^{3+} and Pr^{4+}.

The oxidation and reduction processes in the praseodymium pyrochlores and fluorite

In the $Pr_2Zr_2O_7$, $Pr_2(Zr_{2-x}Pr_x)O_{7-x/2}$, and $Pr_2(Zr_{2-x}Pr_x)O_{7-x/2}$ (x = 0.1) pyrochlore solid solution the oxidation process is possible at the higher temperatures:

$$Pr^{3+} + h^{\bullet} \rightarrow Pr^{4+} \quad (4)$$

It starts at T ~ 270 °C [15]. The rate of this process (Eq. (4)) is determined by the oxidation potential E^oPr^{3+}/Pr^{4+} = 2.86–3.2 V. This potential is significantly higher for the Pr^{3+}/Pr^{4+} pair than for Ce^{3+}/Ce^{4+} pair (E^oCe^{3+}/Ce^{4+} = 1.44–1.7 V). Indeed, in the $Ce_2Zr_2O_7$ pyrochlore the oxidation process takes place at room temperature [14], while in $Pr_2(Zr_{2-x}Pr_x)O_{7-x/2}$ and $Pr_2(Zr_{2-x}Pr_x)O_{7-x/2}$ (x = 0, 0.1) this process does not occur at room temperature due to the high oxidation potential. The XPS data for the praseodymium pyrochlores (Fig. 2, curves 1–3) confirm this result (Section 3.2).

Above 270 °C, this process is enhanced. In Ref. [15] the retention of pyrochlore structure and oxidation of Pr^{3+} to Pr^{4+} in $Pr_{2-x}Ca_xZr_2O_7$ (x = 0, 0.075, 0.1) in air at higher temperatures were inferred from thermogravimetry and in situ high temperature XRD data. In the low temperature region (270–500 °C), the oxidation process represented by Eq. (4) is possible for the Pr_3ZrO_x fluorite as well. However, it is known that Pr^{4+} start to reduce to Pr^{3+} at the temperatures T ≥ 500 °C, but nearly all of the Pr^{4+} ~80% is converted to Pr^{3+} above 1000 °C [23,34]. Consider now the possible reduction of Pr^{4+} in the $Pr_2(Zr_{2-x}Pr_x)O_{7-x/2}$ (x = 0.1) pyrochlore and Pr_3ZrO_x fluorite solid solutions using TG data obtained in He.

According to literature data [23,34] the reduction process should take place at temperatures 500 ≤ T ≤ 1100 °C in Pr_3ZrO_x fluorite, but no or weak reduction occurs in the $Pr_2(Zr_{2-x}Pr_x)O_{7-x/2}$ (x = 0.1) pyrochlore phase with a very small percent of Pr^{4+} on the Pr^{3+} sites of the pyrochlore structure [28]. Fig. 3 presents TG data of the Pr_3ZrO_x (Fig. 3, curve 1) and $Pr_2(Zr_{2-x}Pr_x)O_{7-x/2}$ (x = 0.1) (Fig. 3, curve 2) in He in the temperature interval 25–1100 °C. The weight loss of Pr_3ZrO_x in He up to 500 °C is related to the physical water release. The reduction of Pr^{4+} to Pr^{3+} in the Pr_3ZrO_x (Fig. 3, insert, curve 1) was accompanied by the formation of oxygen, as was evidenced by an increase in ion current at *m*/*z* = 32 at T ~ 600 °C and T > 800 °C. This extent of process was very low in the $Pr_2(Zr_{2-x}Pr_x)O_{7-x/2}$ (x = 0.1) pyrochlore at T > 800 °C (Fig. 3, insert, curve 2). This result confirms the existence of Pr^{4+} in the Pr_3ZrO_x. In the $Pr_2(Zr_{2-x}Pr_x)O_{7-x/2}$ (x = 0.1) pyrochlore praseodymium has predominantly 3+ oxidation state.

Michel et al. [28] determined the oxidation state of praseodymium in a fluorite phase of composition 60% Pr_2O_3 – 40% ZrO_2 (Pr_3ZrO_x) after slow cooling from 800 °C and rapid quenching from the same temperature. The oxidation state of praseodymium was found to be 3.15 in the quenched sample and 3.34 in the slowly cooled sample. After slow cooling, Pr_3ZrO_x contained more Pr^{4+} and more oxygen. We have calculated the parameter of Pr_3ZrO_x fluorite after slow cooling from 800 °C and rapid quenching (in liquid N_2) from the same temperature using Rietveld refinement (Fig. 1, d, e). The parameter of the cubic cell a was found to be 5.4297(1) Å in the quenched sample and 5.41874(9) Å in the slowly cooled sample. This result confirms the increasing of Pr^{3+}/Pr^{4+} ratio at high temperature (800 °C) and the decreasing of this ratio down to room temperature in Pr_3ZrO_x fluorite.

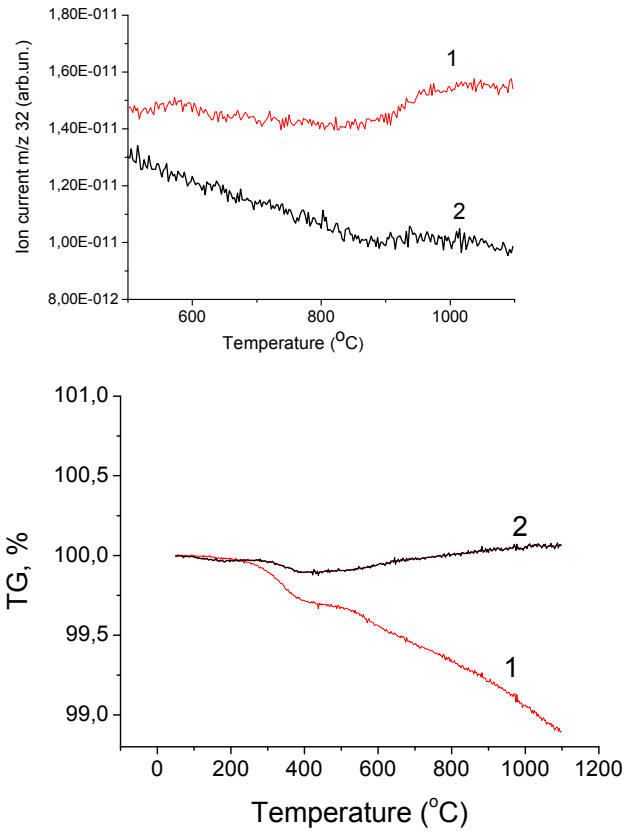

Fig. 3 – TG data of (1) Pr_3ZrO_x and (2) $Pr_2(Zr_{2-x}Pr_x)O_{7-x/2}$ (x = 0.1) in He in the temperature interval 25–1100 °C. Insert: ion current for *m*/*z* = 32 (oxygen) during heating of (1) Pr_3ZrO_x and (2) $Pr_2(Zr_{2-x}Pr_x)O_{7-x/2}$ (x = 0.1) in an inert atmosphere (He).

Thermomechanical properties of the $(Pr_{2-x}Zr_x)Zr_2O_{7+x/2}$ ($x = 0.15$), $Pr_2Zr_2O_7$, and $Pr_2(Zr_{2-x}Pr_x)O_{7-x/2}$ ($x = 0.1$) pyrochlores and Pr_3ZrO_x fluorite

Fig. 4 and Table 3 show thermomechanical data obtained in air for the potential ionic interstitial conductor $(Pr_{2-x}Zr_x)Zr_2O_{7+x/2}$ with x = 0.15 (pyrochlore structure) (Fig. 4 curve 1); the pure pyrochlore $Pr_2Zr_2O_7$ (Fig. 4 curve 2); the potential vacancy conductor $Pr_2(Zr_{2-x}Pr_x)O_{7-x/2}$ with x = 0.1 (pyrochlore structure) (Fig. 4 curve 3); and the Pr-rich fluorite solid solution Pr_3ZrO_x (Fig. 4 curve 4). The curves can be divided into two groups. One group is formed by the curves of the pyrochlore materials, and the other, by the curve of the Pr_3ZrO_x fluorite phase. The TEC of the fluorite phase Pr_3ZrO_x considerably deviates from linearity above 500 °C (Fig. 4, curve 4). In the range 540–626 °C, the TEC of the pyrochlores also exhibits nonlinear behavior, but the deviation from linearity is markedly smaller (Table 3). In all cases, the TEC is on the order of $(10–11.5) \times 10^{-6}\ K^{-1}$ below the break. At higher temperatures, fluorite Pr_3ZrO_x has the largest TEC, $22 \times 10^{-6}\ K^{-1}$, whereas the TEC of the pyrochlores is $(15–18) \times 10^{-6}\ K^{-1}$.

Previously, similar nonlinearity was observed in the TEC of doped and undoped $Dy_2Ti_2O_7$ pyrochlore at 700 °C, which was attributed to the antiferroelectric phase transition in the oxygen sublattice of pyrochlore-based solid solutions at this temperature [35]. Thus, oxygen mobility in both undoped and Ca-doped $Ln_2Ti_2O_7$ pyrochlores changes above 700 °C [35]. A similar effect was observed earlier at ~500 °C in Sc_2O_3-doped ZrO_2 with fluorite structure [36]. In the Sc_2O_3 doped ZrO_2 this effect is related to the ferroelastic ↔ ferroelectric phase transition from rhombohedral to the cubic phase [36]. We assume the phase transformation in our pyrochlore samples, which is associated with changes in the oxygen sublattice of $(Pr_{2-x}Zr_x)Zr_2O_{7+x/2}$ (x = 0.15), $Pr_2Zr_2O_7$, and $Pr_2(Zr_{2-x}Pr_x)O_{7-x/2}$ (x = 0.1) in the range 540–626 °C (Table 3). The fluorite-like phase – disordered pyrochlore phase transition near 800 °C was observed recently by Payne at al. [37] for the neodymium zirconate $Nd_2Zr_2O_7$.

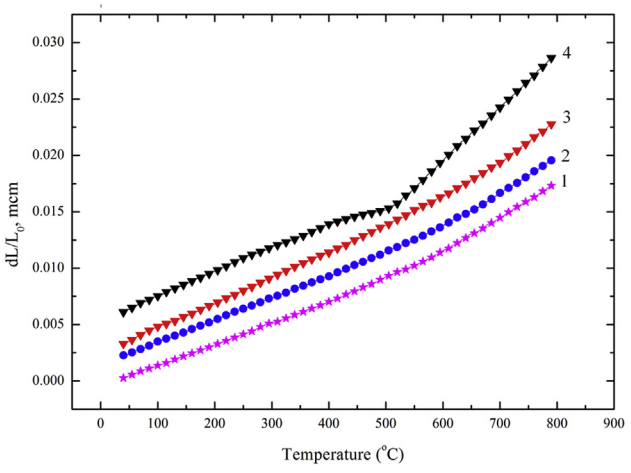

Fig. 4 – TMA curve for (1) $(Pr_{2-x}Zr_x)Zr_2O_{7+x/2}$ (x = 0.15), (2) $Pr_2Zr_2O_7$, (3) $Pr_2(Zr_{2-x}Pr_x)O_{7-x/2}$ (x = 0.1) and (4) Pr_3ZrO_x acquired during second heating of the samples from room temperature up to 800 °C. The curves are offset along the ordinate for clarity.

According to Rietveld data (Section 3.1), the structure of Pr_3ZrO_x is the most similar to the fluorite structure, with a unit-cell parameter of 5.41874(9) Å, which is close to that of $PrO_{2-\delta}$: 5.392 Å (JCPDS PDF-2 24-1006). At the room temperature Pr_3ZrO_x is deep black in color, which suggests high Pr^{4+} content, in agreement with the above XPS data (Fig. 2). In both pyrochlore and fluorite phases, the eight-coordinate ionic radius of Pr^{3+} is 1.126 Å and that of Pr^{4+} is considerably smaller: 0.96 Å [38]. What is then the cause of the marked deviation of the TEC of fluorite Pr_3ZrO_x from linearity above 500 °C? In a number of reports [23–25], the concept of chemical expansion was proposed for Pr-containing potential SOFC cathodes: $Pr_xCe_{1-x}O_{2-\delta}$ (x = 0, 0.01, 0.1, 0.2). Above 500 °C, the deviation of their TEC from linearity was found to increase with increasing Pr content. The oxygen loss from the $Pr_xCe_{1-x}O_{2-\delta}$ (x = 0, 0.01, 0.1, 0.2) lattice during high-temperature heat treatment or holding under reducing conditions follows the scheme [23].

$$O_O^x + 2Pr_{Ce}^x \leftrightarrow V_O^{\bullet\bullet} + 2\,Pr_{Ce}' + ½\,O_2(g), \tag{5}$$

where Pr_{Ce}^x – (Pr^{4+}) and Pr_{Ce}' – (Pr^{3+}) are Pr cations on the Ce site. At 700 °C and $P_{O2} > 10^{-18}$ atm, the electroneutrality condition has the form

$$[Pr_{Ce}'] \sim 2[V_O^{\bullet\bullet}]. \tag{6}$$

Thus, the most likely cause of the chemical expansion of the Pr^{4+}-containing Pr_3ZrO_x sample under consideration is the increase in ionic radius in going from Pr^{4+} to Pr^{3+} during heating in air above 500 °C. The Kröger–Vink equations in this case have the form

$$O_O^x + 2Pr_{Pr}^x \leftrightarrow V_O^{\bullet\bullet} + 2\,Pr_{Pr}' + ½\,O_2\,(g), \tag{7}$$

where $Pr_{Pr}^x = Pr^{4+}$ and $Pr_{Pr}' = Pr^{3+}$.

Similarly, at T > 500 °C and $P_{O2} > 10^{-18}$ atm the electroneutrality condition has the form

$$[Pr_{Pr}'] \sim 2\,[V_O^{\bullet\bullet}]. \tag{8}$$

We believe that, during high-temperature annealing of Pr_3ZrO_x under oxidizing conditions in air, partial reduction of Pr^{4+} to Pr^{3+} is possible (Fig. 3) and that the expansion of the cubic cell due to the presence of the larger cation Pr^{3+} (Section 3.3) may be responsible for the deviation of the TEC from linearity above 500 °C (Table 3).

Transport properties of the $(Pr_{2-x}Zr_x)Zr_2O_{7+x/2}$ ($x = 0.15$), $Pr_2Zr_2O_7$, and $Pr_2(Zr_{2-x}Pr_x)O_{7-x/2}$ ($x = 0.1$) pyrochlores and Pr_3ZrO_x fluorite

Transport properties were evaluated by impedance spectroscopy in air as functions of temperature and oxygen partial pressure at isothermal conditions. Fig. 5 shows typical impedance spectra at 300 (Fig. 5 a) and 700 °C (Fig. 5 b). These spectra show that it is very easy to determine the total conductivity of each sample. However, deconvolution into bulk and grain boundary contributions is impossible, at least at high temperatures, ~700 °C. At low temperatures (Fig. 5a), it is

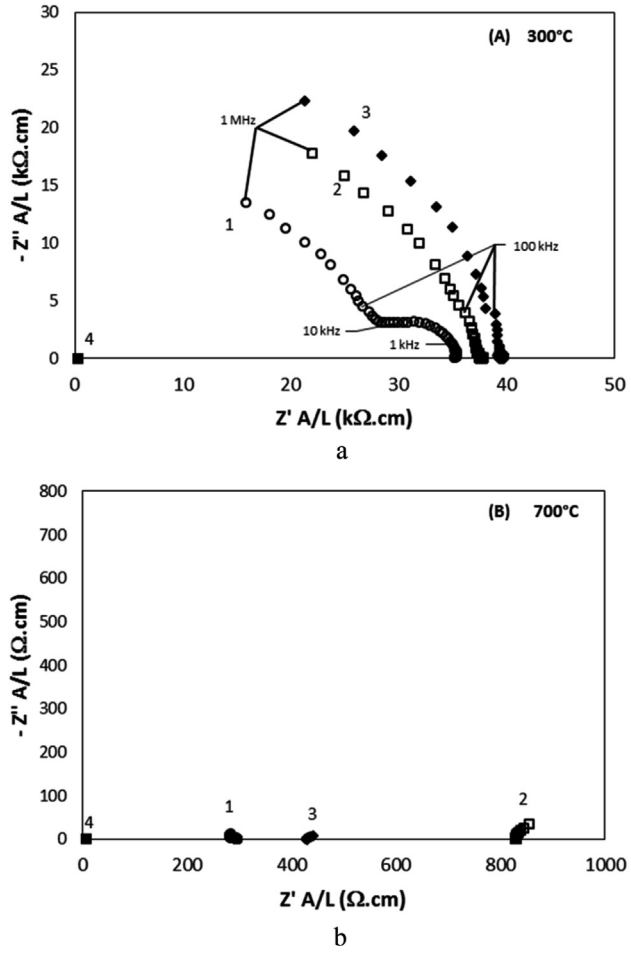

Fig. 5 – Impedance spectra for (1) $(Pr_{2-x}Zr_x)Zr_2O_{7+x/2}$ ($x = 0.15$), (2) $Pr_2Zr_2O_7$, (3) $Pr_2(Zr_{2-x}Pr_x)O_{7-x/2}$ ($x = 0.1$) and (4) Pr_3ZrO_x at (A) 300 °C and (B) 700 °C.

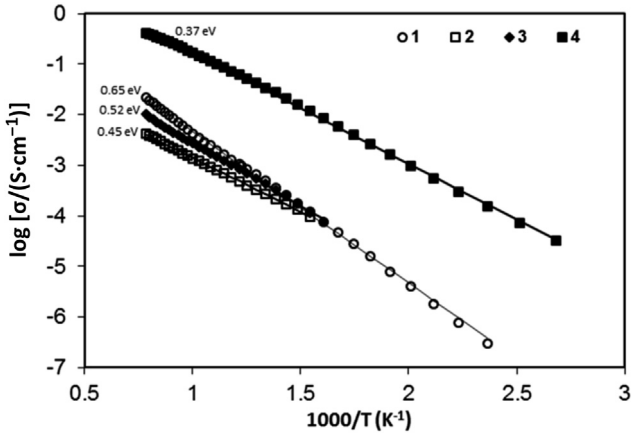

Fig. 6 – Arrhenius plot for (1) $(Pr_{2-x}Zr_x)Zr_2O_{7+x/2}$ ($x = 0.15$), (2) $Pr_2Zr_2O_7$, (3) $Pr_2(Zr_{2-x}Pr_x)O_{7-x/2}$ ($x = 0.1$), and (4) Pr_3ZrO_x compositions in air. Activation energy values are written along each curve.

possible to see a small semicircle related to the grain boundary contribution for $(Pr_{2-x}Zr_x)Zr_2O_{7+x/2}$ ($x = 0.15$), but it was impossible to get this information to the other compositions, and so, total conductivity (bulk + grain boundary) was used to evaluate the electrical properties of these materials. The Arrhenius plot of total conductivity for Pr_3ZrO_x in air (Fig. 6 curve 4) demonstrates that this fluorite material has very high conductivity. The activation energies founded for each composition it will be discuss below.

Fig. 7 shows log–log plots of total conductivity vs. oxygen partial pressure for the $(Pr_{2-x}Zr_x)Zr_2O_{7+x/2}$ ($x = 0.15$) interstitial oxide ion conductor (Fig. 7, curve 1), $Pr_2Zr_2O_7$ ordered pyrochlore phase (Fig. 7, curve 2), $Pr_2(Zr_{2-x}Pr_x)O_{7-x/2}$ ($x = 0.1$) oxygen vacancy conductor (Fig. 7, curve 3), and Pr_3ZrO_x Pr-rich fluorite solid solution (Fig. 7, curve 4) at 1000 °C. The highest contribution of the oxide ion conductivity was found in the $(Pr_{2-x}Zr_x)Zr_2O_{7+x/2}$ ($x = 0.15$) interstitial conductor: 3×10^{-2} S/cm at 1000 °C (Fig. 7, curve 1) and 6×10^{-3} S/cm at 700 °C (Fig. 6, curve 1). The ordered pyrochlore phase $Pr_2Zr_2O_7$ (Tables 1 and 2) had the lowest oxide ion conductivity contribution among the materials studied: ~1×10^{-4} S/cm at 1000 °C (Fig. 7, curve 2). The $Pr_2(Zr_{2-x}Pr_x)O_{7-x/2}$ ($x = 0.1$) oxygen vacancy conductor had intermediate oxide ion conductivity contribution: 3×10^{-3} S/cm at 1000 °C (Fig. 7, curve 3). A similar situation was observed previously for $Nd_{2\pm x}Zr_{2\pm x}O_{7\pm\delta}$ solid solutions [26,27]: the highest conductivity was found in the $(Nd_{2-x}Zr_x)Zr_2O_{7+x/2}$ ($x = 0.2, 0.32, 0.39$) interstitial conductors, up to 2.16×10^{-3} S/cm at 700 °C, and the lowest, in the ordered pyrochlore phase $Nd_2Zr_2O_7$, ~5×10^{-5} S/cm at 700 °C. Note that the $(Pr_{2-x}Zr_x)Zr_2O_{7+x/2}$ ($x = 0.15$) interstitial conductor was also found to have the widest range of predominantly oxide-ion conduction: from 10^{-10} to 10^2 Pa (Fig. 7, curve 1). Under both reducing and mild oxidizing conditions, $(Pr_{2-x}Zr_x)Zr_2O_{7+x/2}$ with $x = 0.15$ is a purely ionic conductor (Fig. 7, curve 1). In $Pr_2Zr_2O_7$ and $Pr_2(Zr_{2-x}Pr_x)O_{7-x/2}$ with $x = 0.1$, p-type conductivity prevails at 1000 °C and $P_{O2} > 10^{-5}$ Pa. At 1000 °C in air (for high oxygen partial pressures) all pyrochlores are mixed, ionic–electronic conductors in which electronic conduction prevails. Measurements preformed at 900, 800 and 700 °C,

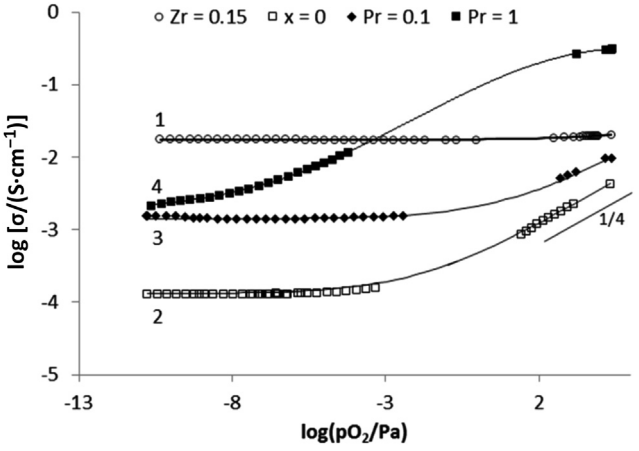

Fig. 7 – Electrical conductivity versus oxygen partial pressure for (1) $(Pr_{2-x}Zr_x)Zr_2O_{7+x/2}$ ($x = 0.15$), (2) $Pr_2Zr_2O_7$, (3) $Pr_2(Zr_{2-x}Pr_x)O_{7-x/2}$ ($x = 0.1$), and (4) Pr_3ZrO_x compositions at 1000 °C.

confirmed the same trend observed at 1000 °C, and due to YSZ sensor limitations, measurements below 700 °C were not performed.

The p-type conductivity of $Pr_2Zr_2O_7$ (Fig. 7, curve 2) and $Pr_2(Zr_{2-x}Pr_x)O_{7-x/2}$ with x = 0.1 (Fig. 7, curve 3) at high oxygen partial pressures is controlled by intrinsic anti-Frenkel defects and by extrinsic Pr excess, respectively. The corresponding electroneutrality conditions are given by:

$$\left[V_O^{\bullet\bullet}\right] = \left[O_i''\right] \tag{9}$$

$$2\left[V_O^{\bullet\bullet}\right] = \left[Pr'_{Zr}\right] \tag{10}$$

These equations combined with the band–band transfer and with the atmosphere equilibrium, can be used to calculate the electronic hole concentration dependence as a function of the oxygen partial pressure:

$$0 \leftrightarrow e' + h^{\bullet} \tag{11}$$

$$K_e = np \tag{12}$$

$$O_O^x \leftrightarrow 1/2O_2 + V_O^{\bullet\bullet} + 2'_e \tag{13}$$

$$K_{ox} = \left[V_O^{\bullet\bullet}\right] n^2 pO_2^{1/2} \tag{14}$$

$$p = Ke\left(\left[V_O^{\bullet\bullet}\right]/K_{ox}\right)^{1/2} pO_2^{1/4} \tag{15}$$

As predict by Eqs. (9) and (10), the oxygen vacancy concentration are fixed, or by the anti-Frenkel defect equilibrium constant or by the non-stoichiometry, resulting in a ¼ dependence of the p-type conductivity with the oxygen partial pressure, as observed in Fig. 7 (curves 2 and 3).

According to Table 1 and Eqs. (2) and (3), the interstitial conductor $(Pr_{2-x}Zr_x)Zr_2O_{7+x/2}$ (x = 0.15) contains no oxygen vacancies but contains oxygen interstitials. The vacancy conductor $Pr_2(Zr_{2-x}Pr_x)O_{7-x/2}$ (x = 0.1) has partially filled oxygen vacancies and no interstitials. The interstitial oxygen ion conductor $(Pr_{2-x}Zr_x)Zr_2O_{7+x/2}$ (x = 0.15) has a larger percentage of anti-structure pairs (3%) and higher oxygen ion conductivity. However, the anti-structure pairs do not affect the electroneutrality of the material, because the charge in each position is compensated and so, we do not expect significant effects on electrical conductivity, unless due to some changes in carrier mobility [39].

It was of particular interest to study fluorite (Pr_3ZrO_x) [20], which had an anomalously high conductivity in air: 0.17 S/cm at 700 °C (0.5 S/cm at 1000 °C). The present results (Fig. 7, curve 4) demonstrate that in air this material is a p-type electronic conductor and that its ionic conductivity prevails at oxygen partial pressures below 10^{-10} Pa, i.e. under highly reducing conditions. Its conductivity approaches the oxide ion conductivity of the $Pr_2(Zr_{2-x}Pr_x)O_{7-x/2}$ (x = 0.1) oxygen vacancy conductor: 4×10^{-3} S/cm at 1000 °C.

According to Rietveld data, Pr_3ZrO_x and $PrO_{2-\delta}$ are close in unit-cell parameters. In fluorite Pr_3ZrO_x, a lot of praseodymium cations at room temperature are in 4+ valence state (Pr^{4+}) (Section 3.2, Fig. 2 and Section 3.3). The co-existence of this two valent states can originate electron hopping between Pr^{3+} and Pr^{4+} positions. The shape of the oxygen partial pressure dependence for Pr_3ZrO_x (Fig 7, curve 4) with fluorite type structure, suggests that the conductivity reaches a maximum, in agreement with the small polaron mechanism for the conductivity, which should occur for $Pr^{3+}/Pr^{4+} = 1$. The oxidation state of praseodymium in that case should be 3.5 at the measurement temperature. For fluorite Pr_3ZrO_x the Pr^{3+}/Pr^{4+} ratio at high temperature ~800 °C is 3.15 [28]. Then it is possible only weak small polaron contribution to the conductivity of fluorite Pr_3ZrO_x. This type of conductivity was also found by Bishop et al. [34] for Pr-doped cerium oxide, also with the fluorite structure.

The stoichiometric composition $Pr_2Zr_2O_7$ (Fig. 7, curve 2) also shows an evident increase of conductivity at high oxygen partial pressures. However, XPS measurements only reveal the presence of Pr^{3+}, without any traces of Pr^{4+}, at room temperature, and it is not expected a transition from Pr^{3+} to Pr^{4+} at the measurement temperature (1000 °C). So, it is not realistic to consider hoping mechanism for the electronic conductivity founded in these compositions in oxidizing conditions. Note that in the fluorite Pr-doped cerium oxide, the Pr^{3+} ion is at Ce^{4+} position, with trend to oxidize, and otherwise, in the pyrochlore $Pr_2Zr_2O_7$, the Pr^{3+} is in his natural position. Consequently, we suggest that the p-type conductivity is due to the band–band transfer, in agreement with Eqs. (11) and (12), resulting in a ¼ dependence with the oxygen partial pressure, as predict by Eq. (15).

Based on XPS results, similar conclusions can be made for $Pr_2(Zr_{2-x}Pr_x)O_{7-x/2}$ (x = 0.1) (Fig. 7, curve 3), i.e., the onset on the electronic conductivity at high oxygen partial pressures is due the p-type conductivity in the valence band.

For $(Pr_{2-x}Zr_x)Zr_2O_{7+x/2}$ with x = 0.15 (Fig. 7, curve 1) the p-type and the ionic conductivities, for high oxygen partial pressures, have the same order of magnitude and so, in this conditions, we have a mixed conductor.

The activation energies obtained in air, Fig. 6, are in agreement with the conduction mechanism founded. Taking into account the ionic conductivity for each composition (low oxygen partial pressures conductivities) between 700 and 1000 °C, we get an activation energy of about 1 eV for all pyrochlores and 1.5 eV for the fluorite composition. Differences between activations energies in Fig. 6 are related with the mixed nature of the conduction of these materials. The activation energy increases with the increase of the ionic component weight.

Conclusions

We have investigated the effect of Pr^{3+}/Pr^{4+} ratio on the oxygen ion transport and thermomechanical properties of the solid solutions in the $ZrO_2 - Pr_2O_3$ binary oxide system. The solid solutions were prepared through coprecipitation followed by pressing and firing of the green compacts in air at 1550 °C. The Pr^{3+}/Pr^{4+} ratio was shown to decrease across the above series in going from pyrochlores to fluorite, leading to changes in the conductivity type and color of the solid solutions and the behavior of their TEC. In particular, the $(Pr_{2-x}Zr_x)Zr_2O_{7+x/2}$ (x = 0.15) pyrochlore solid solution is a purely interstitial oxide ion conductor (3×10^{-2} S/cm at 1000 °C) in a wide range of oxygen partial pressures: from 10^{-10} to 10^2 Pa.

However in air this material is mixed, ionic–electronic conductor. In the $Pr_2Zr_2O_7$ and $Pr_2(Zr_{2-x}Pr_x)O_{7-x/2}$ ($x = 0.1$) pyrochlores, p-type conduction prevails at 1000 °C and $P_{O2} > 10^{-5}$ Pa, i.e. in air these materials are mixed, ionic–electronic conductors in which hole conduction prevails. For $P_{O2} < 10^{-5}$ Pa, the 1000 °C oxide ion conductivity of pyrochlore $Pr_2Zr_2O_7$ and that of the pyrochlore $Pr_2(Zr_{2-x}Pr_x)O_{7-x/2}$ ($x = 0.1$) oxygen vacancy conductor are 1×10^{-4} and 3×10^{-3} S/cm, respectively, and are lower than that of $(Pr_{2-x}Zr_x)Zr_2O_{7+x/2}$ with $x = 0.15$. Fluorite Pr_3ZrO_x is a p-type electronic conductor with a 1000 °C conductivity of 0.5 S/cm. However the weak small polaron contribution may exist in this fluorite. The considerable deviation of the TEC of Pr_3ZrO_x fluorite from linearity above 500 °C is due to partial reduction of Pr^{4+}, which leads to an increase in the unit-cell parameter and, hence, in the dimensions of the sample. The reduction of Pr^{4+} to Pr^{3+} in the Pr_3ZrO_x fluorite above 500 °C has been identified using TG and mass spectrometry in a He atmosphere.

Acknowledgment

This work was supported by the Russian Foundation for Basic Research (grant no. 13-03-00680, 16-03-00143) and in part by M.V. Lomonosov Moscow State University (Program of Development).

REFERENCES

[1] Subramanian MA, Aravamudan G, Subba Rao GV. Oxide pyrochlores–A review. Prog Solid State Chem 1983;15:55–143.
[2] Chakoumakos BC. Systematics of the pyrochlore structure type, ideal A2B2X6Y. J Solid State Chem 1984;53:120–9.
[3] Wilde PJ, Catlow CRA. Defects and diffusion in pyrochlore structured oxides. Solid State Ionics 1998;112:173–83.
[4] Wuensch BJ, Eberman KW, Heremans C, Ku EM, Onnerud P, Yeo EME, et al. Connection between oxygen-ion conductivity of pyrochlore fuel-cell materials and structural change with composition and temperature. Solid State Ionics 2000;129:111–33.
[5] Kramer SA,Tuller HL. A novel titanate-based oxygen ion conductor $Gd_2Ti_2O_7$. Solid State Ionics 1995;82:15–23.
[6] Kramer SA, Spears MA, Tuller HL. Conduction in titanate pyrochlores: role of dopants. Solid State Ionics 1994;72:59–66.
[7] Shlyakhtina AV, Shcherbakova LG. New solid electrolytes of the pyrochlore family. Russ J Electrochem 2012;1:1–25.
[8] Shlyakhtina AV. Morphotropy, isomorphism and polymorphism of $Ln_2M_2O_7$ (Ln = La, Lu, Y, Sc; M = Ti, Zr, Hf, Sn) oxides. Cryst Rep 2013;58:548–62.
[9] Gill JK, Pandey OP, Singh K. Role of sintering temperature on thermal, electrical and structural properties of $Y_2Ti_2O_7$ pyrochlores. Int J Hydrogen Energy 2011;36:14943–7.
[10] Gill JK, Pandey OP, Singh K. Ionic conductivity, structural and thermal properties of Ca^{2+} doped $Y_2Ti_2O_7$ pyrochlores for SOFC. Int J Hydrogen Energy 2012;37:3857–64.
[11] Kharton VV, Naumovich EN, Vecher AA. Research on the electrochemistry of oxygen ion conductors in the former Soviet Union. I. ZrO_2-based ceramic materials. J Solid State Electrochem 1999;3:61–81.
[12] Savvin SN, Shlyakhtina AV, Belov DA, Ruiz-Morales JC, Shcherbakova LG, Nunez P. Stability of $(Ln_{0.8}Ca_{0.1}Ln'_{0.1})_2Ti_2O_{7-\delta}$ (Ln = Dy, Yb; Ln' = Ce, Tb) and $(Tb_{0.9}Ca_{0.1})_2Ti_2O_{7-\delta}$ pyrochlores under redox conditions. Solid State Ionics 2012;225:457–63.
[13] Hui Z, Nicolas G, Francoise V, Michele P. Preparation and electrical properties of a pyrochlore-related $Ce_2Zr_2O_{8-x}$ phase. Solid State Ionics 2003;160:317–26.
[14] Achary SN, Sali SK, Kulkarni NK, Krishna PSR, Shinde AB, Tyagi AK. Intercalation/deintercalation of oxygen: a sequential evolution of phases in Ce_2O_3/CeO_2–ZrO_2 pyrochlores. Chem Mater 2009;21:5848–59.
[15] Vasundhara K, Achary SN, Tyagi AK. Structure, thermal and electrical properties of calcium doped pyrochlore type praseodymium zirconate. Int J Hydrogen Energy 2015;40:4252–62.
[16] Arsentiev PA, Glushkova VB, Evdokimov AA, Keler EK, Kravchenko VB, Kravchinskaya MV, et al. Rare-earth compounds: zirconates, hafnates, tantalates, and antimonates. In: Khimiya redkikh elementov (Chemistry of rare elementes). Moscow: Nauka; 1985.
[17] Shlyakhtina AV, Knotko AV, Boguslavskii MV, Stefanovich SYu, Kolbanev IV, Larina LL, et al. Effect of non-stoichiometry and synthesis temperature on the structure and conductivity of $Ln_{2+}xM_{2-x}O_{7-x/2}$ (Ln = Sm–Gd; M = Zr, Hf; x = 0–0.286). Solid State Ionics 2007;178:59–66.
[18] Tsipis EV, Shlyakhtina AV, Shcherbakova LG, Kolbanev IV, Kharton VV, Vyshatko NP, et al. Mechanically-activated synthesis and mixed conductivity of $TbMO_{4-\delta}$ (M = Zr, Hf) ceramics. J Electroceram 2003;10:153–64.
[19] Holtappels P, Poulsen FW, Mogensen M. Electrical conductivities and chemical stabilities of mixed conducting pyrochlores for SOFC applications. Solid State Ionics 2000;135:675–9.
[20] Belov DA, Shlyakhtina AV, Abrantes JCC, Chernyak SA, Gasymova GA, Karyagina OK, et al. Electrochemical behavior of the pyrochlore- and fluorite-like solid solutions in the Pr_2O_3–ZrO_2 system. Part I Solid State Ionics 2015;271:79–85.
[21] Poulsen FW, Glerup M, Holtappels P. Structure, Raman spectra and defect chemistry modelling of conductive pyrochlore oxides. Solid State Ionics 2000;135:595–602.
[22] Shukla R, Vasundhara K, Krishna PSR, Shinde AB, Sali SK, Kulkarni NK, et al. High temperature structural and thermal expansion behavior of pyrochlore-type praseodymium zirconate. Int J Hydrogen Energy 2015;40:15672–8.
[23] Bishop SR, Tuller HL, Kuru Y, Yildiz B. Chemical expansion of nonstoichiometric $Pr_{0.1}Ce_{0.9}O_{2-\delta}$: correlation with defect equilibrium model. J Eur Ceram Soc 2011;31:2351–6.
[24] Kuru Y, Bishop SR, Kim JJ, Yildiz B, Tuller HL. Chemomechanical properties and microstructural stability of nanocrystalline Pr-doped ceria: an in situ X-ray diffraction investigation. Solid State Ionics 2011;193:1–4.
[25] Tuller HL, Bishop SR, Chen D, Kuru Y, Kim J-J, Stefanik TS. Praseodymium doped ceria: model mixed ionic electronic conductor with coupled electrical, optical, mechanical and chemical properties. Solid State Ionics 2012;225:194–7.
[26] Shlyakhtina AV, Belov DA, Knotko AV, Avdeev M, Kolbanev IV, Vorobieva GA, et al. Oxide ion transport in $(Nd_{2-x}Zr_x)Zr_2O_{7+\delta}$ electrolytes by an interstitial mechanism. J Alloys Compd 2014;603:274–81.
[27] van Dijk T, de Vries KJ, Burggraaf AJ. Electrical conductivity of fluorite and pyrochlore $Ln_xZr_{1-x}O_{2-x/2}$ (Ln = Gd, Nd) solid solutions. Phys Stat Solid A 1980;58:115–25.
[28] Michel D, Perez Y, Jorba M, Collongues R. Etude de la transformation ordre-desordre de la structure fluorite a la structure pyrochlore pour des phases (1–x) $ZrO_{2-x}Ln_2O_3$. Mater Res Bull 1974;9:1457–68.

[29] Rouanet A. Etude des systems zircon-oxyde de prazeodime et zircon-oxyde de terbium a haute temperature. CR Acad Sci C 1968;286:1230–3.
[30] Strekalovskii VN, Volchenkova ZS, Samarina VA. To the study the phase components in the ZrO_2–$PrO_{1.83}$ system. Izv Akad Nauk SSSR, Neorg Mater 1965;7:1372–5.
[31] Hea H, Dai HX, Wong KW, Au CT. $RE_{0.6}Zr_{0.4-x}Y_xO_2$ (RE = Ce, Pr; x = 0, 0.05) solid solutions: an investigation on defective structure, oxygen mobility, oxygen storage capacity, and redox properties. Appl Catal A General 2003;251:61–74.
[32] Hea H, Dai HX, Au CT. Defective structure, oxygen mobility, oxygen storage capacity, and redox properties of RE-based (RE = Ce, Pr) solid solutions. Catal Today 2004;90:245–54.
[33] MYu Sinev, Graham GW, Haack LP, Shelef M. Kinetic and structural studies of oxygen availability of the mixed oxides $Pr_{1-x}M_xO_y$ (M = Ce, Zr). J Mater Res 1996;11:1960–71.
[34] Bishop SR, Stefanik TS, Tuller HL. Electrical conductivity and defect equilibria of $Pr_{0.1}Ce_{0.9}O_{2-\delta}$. Phys Chem Chem Phys 2011;13:10165–73.
[35] Belov DA, Shlyakhtina AV, Stefanovich SYu, Shchegolikhin AN, Knotko AV, Karyagina OK, et al. Antiferroelectric phase transition in pyrochlore-like $(Dy_{1-x}Ca_x)_2Ti_2O_{7-\delta}$ (x = 0, 0.1) high temperature conductors. Solid State Ionics 2011;192:188–94.
[36] Weller M, Khelfaoui F, Kilo M, Taylor MA, Argirusis C, Borchardt G. Defects and phase transitions in yttria- and scandia-doped zirconia. Solid State Ionics 2004;175:329–33.
[37] Payne JL, Tucker MG, Evans IR. From fluorite to pyrochlore: characterisation of local and average structure of neodymium zirconate $Nd_2Zr_2O_7$. J Solid State Chem 2013;205:29–34.
[38] Shannon RD, Prewitt CT. Effective ionic radii in oxides and fluorides. Acta Crystallogr B 1969;25:925–46.
[39] Horovistiz AL, Abrantes JCC, Fagg DP, Frade JR. Effects of Yb:Ti ratio on transport properties of $Yb_{2\pm x}Ti_{2\pm x}O_{7\pm\delta}$. Solid State Ionics 2008;179:1046–9.